Crystallization of Polymer Brushes with Poly(ethylene oxide) Side Chains

Ying Zheng, Merlin L. Bruening, and Gregory L. Baker*

Department of Chemistry, Michigan State University, East Lansing, Michigan 48824

Received February 12, 2007; Revised Manuscript Received June 16, 2007

ABSTRACT: Surface-initiated atom transfer radical polymerization (ATRP) of methoxypoly(ethylene glycol) methacrylate (MPEGMA) macromonomers from immobilized initiators leads to thin films of comblike polymer brushes. The aqueous ATRP procedure results in essentially constant film growth rates and yields coatings with thicknesses as high as 400 nm. Polymers with side chains consisting of 22−23 ethylene oxide repeating units align to form crystalline materials analogous to their nonbrush analogues. However, polarized optical microscopy shows that the polymer films crystallize as two-dimensional spherulites. Both AFM images and reflectance FT-IR spectra of the films are consistent with crystalline lamellae preferentially oriented normal to the surface for brushes with thicknesses above 100 nm. As the film thickness decreases, the favored orientation shifts to crystalline lamellae parallel to the surface, with the PEO side chains oriented perpendicular to the surface. The lamellae orientations are related to polymer−surface interactions as well as to the "comblike" polymeric structure.

Introduction

Thin and ultrathin films are attractive for tailoring surface properties such as wetting and biocompatibility.[1,2] However, a number of studies on polymer films, primarily physically absorbed films deposited on substrates by spin-coating, show that the interactions between the substrate and polymer layers usually lead to physical properties that are different than those of the bulk polymer.[3] For example, the glass transition temperature (T_g) may be enhanced or depressed depending on the film thickness and interfacial interactions,[4] and restriction of chain mobility greatly affects the crystallization of thin films. Polymer morphology,[5−12] degree of crystallinity,[13,14] preferred polymer chain orientation,[5,15] and crystal growth rates[6,13,14,16−21] may vary with film thickness.

Although physical adsorption of films on substrates is a convenient and versatile method for surface modification, physisorbed coatings are often unstable in the presence of good solvents. For this reason, films that are covalently bonded to substrates are being rapidly adopted for the study of thin films. Among such coatings, the properties of polymer brushes are unique to their architecture and have not been explored in detail. For example, the effect of the brush architecture on crystallization could be complicated since the extended chains of densely grafted brushes may preorganize and favor crystallization, while chain entanglements and the restricted mobility of polymer chains in these brushes may retard the crystallization process. Luzinov et al.[22,23] studied the surface morphology of poly(ethylene glycol) (PEG) brushes formed by reacting the end groups of activated PEGs of different molecular masses with a surface primed with poly(glycidyl methacrylate). After PEG grafting, the surface was either partially or totally covered by finger-like crystalline domains, depending on the molecular mass of the constituent PEGs. Since the thicknesses of these films were similar, the variations in crystallite density must be related to the grafting density and the molecular masses of the PEGs.

To further understand the effects of the brush architecture on crystallization, this work examines the crystallization of comblike polymer brushes obtained from atom transfer radical polymerization (ATRP) of methoxypoly(ethylene glycol) methacrylate (MPEGMA) from initiators immobilized on Au surfaces (Scheme 1). ATRP has recently been used to polymerize a variety of hydrophilic monomers in aqueous media,[24−28] and water often dramatically enhances the rate of polymerization.[29−31] Several studies also demonstrated that the use of surface-initiated ATRP at room temperature in aqueous solutions can lead to well-defined and dense polymer brushes.[32−36] In the case of poly(ethylene glycol) methacrylate (PEGMA) and MPEGMA macromonomers, polymerization from surfaces yields comb polymethacrylate brushes with hydrophilic poly(ethylene oxide) (PEO) side chains, as shown in Scheme 1. The side chains of poly(MPEGMA) crystallize when they are sufficiently long, irrespective of the tacticity of the polymer backbone.[37,38] The melting temperature (T_m) of the PEO segments in comb polymers depends on the length of the side chains and ranges from below room temperature to ~65 °C, the T_m of PEO. This range is compatible with self-assembled monolayers of initiators on Au, enabling detailed IR analysis of the structure and orientation of the crystalline PEO side chains of poly(MPEGMA) brushes. In addition to their relevance for understanding crystallization of thin films, poly(MPEGMA) brushes have potentially important applications as gas separation membranes[39] and materials for limiting nonspecific protein adsorption on surfaces,[40,41] and such applications will be directly affected by film crystallinity.[1] Studies of chain crystallization in poly(MPEGMA) brushes complement extensive research on crystallization of bulk PEO,[42,43] physisorbed PEO films on surfaces,[5,6,16] PEO segments in block copolymers,[44,45] and films of PMMA/PEO blends.[11,46,47]

Crystalline PEO comb polymers are usually arranged in a "sandwich" structure, with layers of amorphous backbones alternating with lamellae of crystalline side chains.[37,38,48] In sufficiently thick films, spherulites form, and atomic force microscopy (AFM) makes it possible to observe these spherulites at the lamellar scale. For most ultrathin polymer films that have been studied, crystalline lamellae preferentially orient parallel to the substrate, with the polymer chain axis oriented normal to the surface, as shown in Figure 1.[5,47] The orientation of lamellae may change with the film thickness, and lamellae

* Corresponding author. E-mail: bakerg@msu.edu.

10.1021/ma070367p CCC: $37.00
Published on Web 10/13/2007

Scheme 1. Architecture of a Comblike Poly(MPEGMA) Brush Grown from a Surface

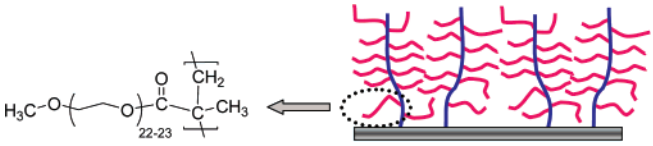

parallel to the surface may give way to perpendicularly oriented lamellae as the film thickness increases. For example, Schönherr et al.[5] studied spin-coated PEO films and reported crystalline lamellae oriented parallel to the substrate in films <300 nm thick and perpendicular lamellae for film thickness >1 μm. The same trend in lamellae orientation was found in semicrystalline polyethylene films[11] and poly(di-*n*-hexylsilane) films.[15] The accepted explanation for these thickness effects is that perpendicular orientation minimizes the energy for the primary nucleation step, and therefore, the same direction is favored for secondary nucleation and crystal growth, resulting in the observed perpendicular lamellae orientation. In ultrathin films, lamellae lying flat on the surface more effectively reduce the surface energy and are favored over perpendicular lamellae.

This paper describes AFM and reflectance FTIR spectroscopy studies of the crystallization of comb poly(MPEGMA) brushes on surfaces. We observed their crystallization as 2-dimensional spherulites and, from reflectance FT-IR spectroscopy, inferred the orientation of the PEO side chains and crystalline lamellae relative to the substrates as a function of film thickness.

Experimental Section

Materials. Methoxypoly(ethylene glycol) methacrylate (MPEGMA, M_w = 1100 g/mol), Cu(I)Br (99.999%), and Cu(II)Br_2 (99.999%) were used as received from Aldrich. 2,2′-Bipyridine (bpy, Aldrich) was recrystallized from hot hexane and sublimed under vacuum at 60 °C. The disulfide initiator [(Br-C$(CH_3)_2$-COO-$(CH_2)_{11}S)_2$] was synthesized using a slightly modified version of a literature procedure.[49] Deionized water (Milli-Q, 18 MΩ cm) was used as the polymerization solvent.

Surface-Initiated Polymerization of MPEGMA. Gold-coated wafers (200 nm of gold sputter-coated on 20 nm of Cr on Si (100) wafers) were UV/O_3-cleaned for 15 min, washed with water and ethanol, and then immersed in a 1 mM ethanolic solution of the disulfide initiator [(Br-C$(CH_3)_2$-COO$(CH_2)_{11}S)_2$] for 24 h to form the self-assembled monolayer. The films were then washed with ethanol, sonicated in ethanol for 1 min, again washed with ethanol, and dried under a stream of N_2. MPEGMA (35 g, 0.032 mol) and 20 mL of Milli-Q water were added to a Schlenk flask and stirred until the MPEGMA was completely dissolved. The flask was then connected to a vacuum line, and the solution was degassed by three freeze−pump−thaw cycles and finally backfilled with Ar. Under a blanket of Ar, Cu(I)Br (0.024 g), Cu(II)Br_2 (0.011 g), and bpy (0.077 g) were added to the solution, and the mixture was stirred for at least 1 h to form a homogeneous dark brown solution. This mixture of monomer and catalyst ([CuBr] = 1 mM, [$CuBr_2$] = 0.3 mM, and [bpy] = 3 mM) was transferred into a N_2-filled glovebag and added to a series of vials, each containing one initiator-modified gold slide. Slides were removed from vials at predetermined times, and the polymer films grown from the gold slides were rinsed sequentially with water, THF, and anhydrous ethanol and then dried under a stream of N_2.

Characterization Methods. Reflectance FT-IR spectroscopy was performed using a Nicolet Magna-IR 560 spectrometer and a PIKE grazing angle (80°) attachment. These measurements employed p-polarized light so only the components of transition dipole moments perpendicular to the surface provide significant absorption peaks in the spectra. The molecular conformations of samples were inferred from IR spectra using the reported assignments of peak absorbances to specific vibrational modes of PEG.[42,43] Film thicknesses were determined using a rotating analyzer ellipsometer (M-44; J.A. Woollam) at an incident angle of 75°. The data were analyzed using WVASE32 software, and the thickness and refractive index determinations were performed on at least three spots on each substrate. The refractive index was fitted along with the film thickness, and the calculated values of the refractive indices were around 1.5. AFM images were measured using the close-contact (oscillating) mode of a Pacific Nanotechnology Nano-R instrument, with the height and phase images recorded simultaneously. The silicon tip had a spring constant of 36 N/m, a tip curvature of 10−20 nm, and a resonant frequency of 286−339 kHz. The scan rate was typically 0.85 Hz.

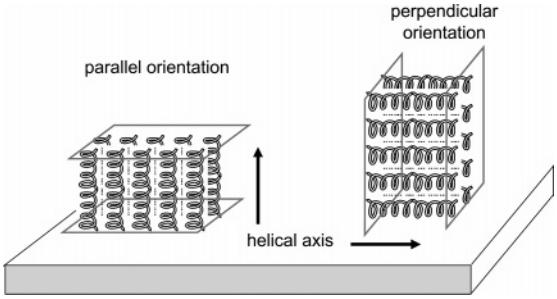

Figure 1. "Parallel" and "perpendicular" orientation of crystalline lamellae on substrates.

Crystallization Studies. The morphology of semicrystalline polymer brushes was examined using a Nikon Optiphot2-POL polarizing optical microscope equipped with a Mettler FP 82 hot-stage and a CCD camera. Samples for isothermal crystallization experiments were heated at 50 °C for 12 h in a vacuum oven to erase the thermal history of the films and then immediately transferred to the hot stage and held at 23 ± 2 °C under a flow of N_2. In nonisothermal crystallization experiments, the samples were loaded into the hot stage, heated to 45 °C (above T_m), cooled at a rate of 1 °C/min to ambient temperature, and then further cooled at a rate of 1 °C/min to ∼5 °C by purging the hot stage with the boil off from liquid N_2. For other experiments, the samples were cooled to ambient temperature in a desiccator under reduced pressure or under N_2.

Results and Discussion

Preparation of Polymer Brushes. Scheme 2 shows the synthetic route used to grow poly(MPEGMA) from gold. Methacrylates containing 4−5, 8−9, and 22−23 ethylene oxide repeat units were polymerized, but only the poly(MPEGMA) with 22−23 PEO units crystallized at room temperature. Research on bulk poly(MPEGMA) shows that the atactic backbone and a portion of the side chains adjacent to the backbone constitute an amorphous phase, and the ethylene oxide chain must exceed a minimum chain length, typically 9−10 ethylene oxide units, to crystallize.[50] The MPEGMA described in the remainder of this document refers to the methacrylate with 22−23 PEO units, unless otherwise specified.

Immobilization of the initiator was confirmed by the appearance of a carbonyl peak in the reflectance FT-IR spectrum of the monolayer (Figure 2a) as well as formation of a 17 ± 2 Å thick film, as measured by ellipsometry. The MPEGMA macromonomer was polymerized from the surface in a nitrogen-filled glovebag using an aqueous solution containing the CuBr/$CuBr_2$/bpy ATRP catalyst. During the first 8 h of the polymerization, the film thickness increased linearly with polymerization time, consistent with a controlled polymerization (Figure 3), but at longer times, the film growth rate decreased, which may reflect reaction of active chain ends with adventitious oxygen in the glovebag. The sterically hindered nature of the macromonomer likely contributes to good control by reducing termination due to bimolecular radical coupling and dispropor-

Scheme 2. Growth of Poly(MPEGMA) Films from Gold Surfaces

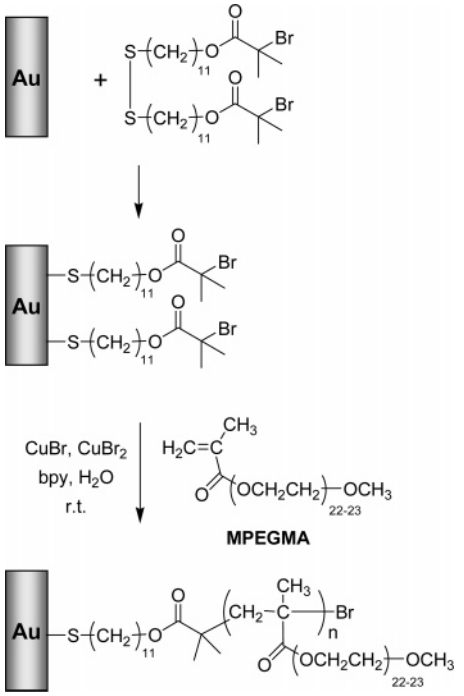

tionation.[29,51] Compared with previous examples of the formation of polymethacrylate brushes with oligo(ethylene glycol) side chains, aqueous ATRP yields 4−10-fold thicker films.[52,53]

Reflectance FT-IR spectra of poly(MPEGMA) films (Figure 2b) measured soon after polymerization show characteristic bands due to C−H stretching (2950−2800 cm^{-1}, not shown), C═O stretching (1740 cm^{-1}), CH_2 bending (∼1460 cm^{-1}), CH_2 wagging (1350 cm^{-1}), overlapping CH_2 twisting modes (∼1300−1240 cm^{-1}), and C−O−C stretching (1150 cm^{-1}). The widths and positions of the absorption peaks are consistent with an amorphous polymer brush. As described below, the evolution of the absorption bands indicates that these films crystallize in air at room temperature.

Morphology of Crystalline Polymer Brushes. The optical microscopy experiments described here provide a qualitative picture of the crystallization behavior as a function of temperature and film thickness. Films stored at room temperature in a desiccator or in open air crystallized, and the mirrorlike finish of as-prepared films developed surface features that were visible to the naked eye. When observed between crossed polarizers, the as-prepared polymer films initially appeared dark (amorphous), but eventually the Maltese cross patterns characteristic of spherulites filled the field of view. The images shown in Figure 4 are from samples annealed at 45 °C and then cooled to either 5 or 10 °C at a rate of 1 °C/min. Since the melting points (T_m) of poly(MPEGMA) films are ∼35−40 °C, the ∼30° supercooling results in a sufficiently high crystallization rate to enable crystallization to be observed in a short period of time.

Panels a and b of Figure 4 show the evolution in polymer morphology for a 240 nm thick film that was heated and then cooled to a specific temperature. After cooling to 10 °C, large and well-defined "spherulites" cover most of the field of view. The domains have similar radii, consistent with nucleation of each domain at comparable times. Eventually, the crystalline domains grow to cover the entire surface. Panel b shows the morphology upon reaching 5 °C. These disclike domains are ∼100 μm in diameter but only 240 nm thick, resulting in an aspect ratio comparable to digital video discs (DVDs). Given their symmetry and disclike geometry, the domains may be viewed as a 2-dimensional slice through the center of a spherulite. Isothermal crystallization at room temperature under N_2 also produced films with spherulitic morphologies.

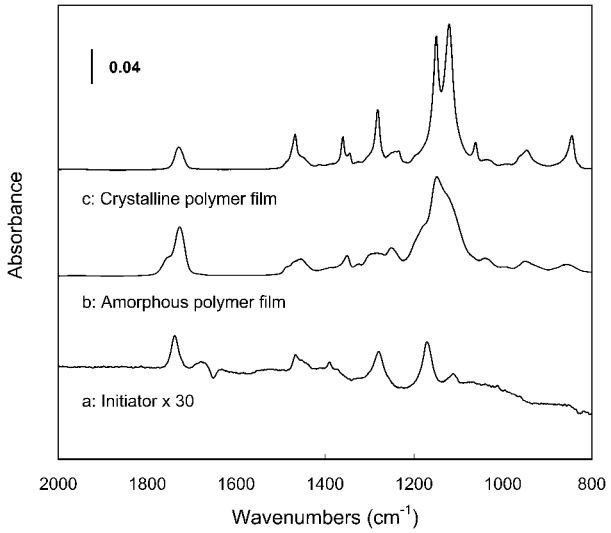

Figure 2. Reflectance FTIR spectra of (a) an initiator monolayer, (b) a 114 nm thick amorphous film of grafted poly(MPEGMA), and (c) a similar poly(MPEGMA) film isothermally crystallized at room temperature. Spectrum b was measured immediately after film synthesis.

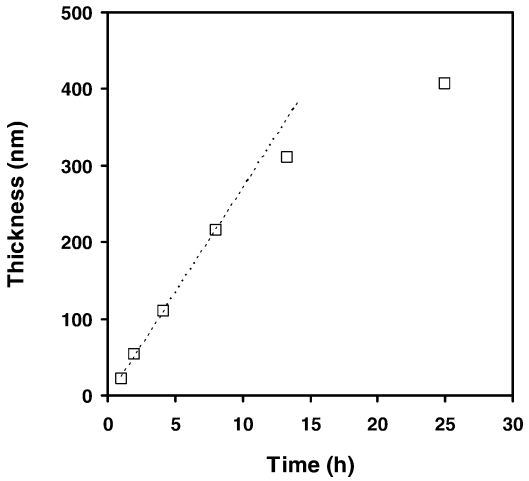

Figure 3. Evolution of film thickness with polymerization time for the room temperature ATRP of MPEGMA from initiators anchored to gold surfaces. Conditions: [CuBr] = 1 mM, [$CuBr_2$] = 0.3 mM, [bpy] = 3 mM, and MPEGMA:H_2O = 2:1 (v/v). The line is a least-squares fit to the first four data points.

Panels b, c, and d of Figure 4 show the effects of film thickness on crystallization. All three samples were imaged immediately after cooling to 5 °C. While the 240 nm film was fully crystallized, some areas of the 148 and 76 nm thick films remained amorphous. The 76 nm thick film appeared as imperfect "spherulites", which are likely the early stages of spherulite formation. These observations show that both the crystalline morphology and crystallization rate depend on the poly(MPEGMA) film thickness.

AFM measurements provided a more detailed view of poly(MPEGMA) surface morphology. Figure 5 shows 2-D and 3-D height images obtained for a 108 nm thick film. These images show the clearly resolved boundary between two spherulitic domains (1) and well-defined lamellae (2) that emanate from the center of the "spherulite".

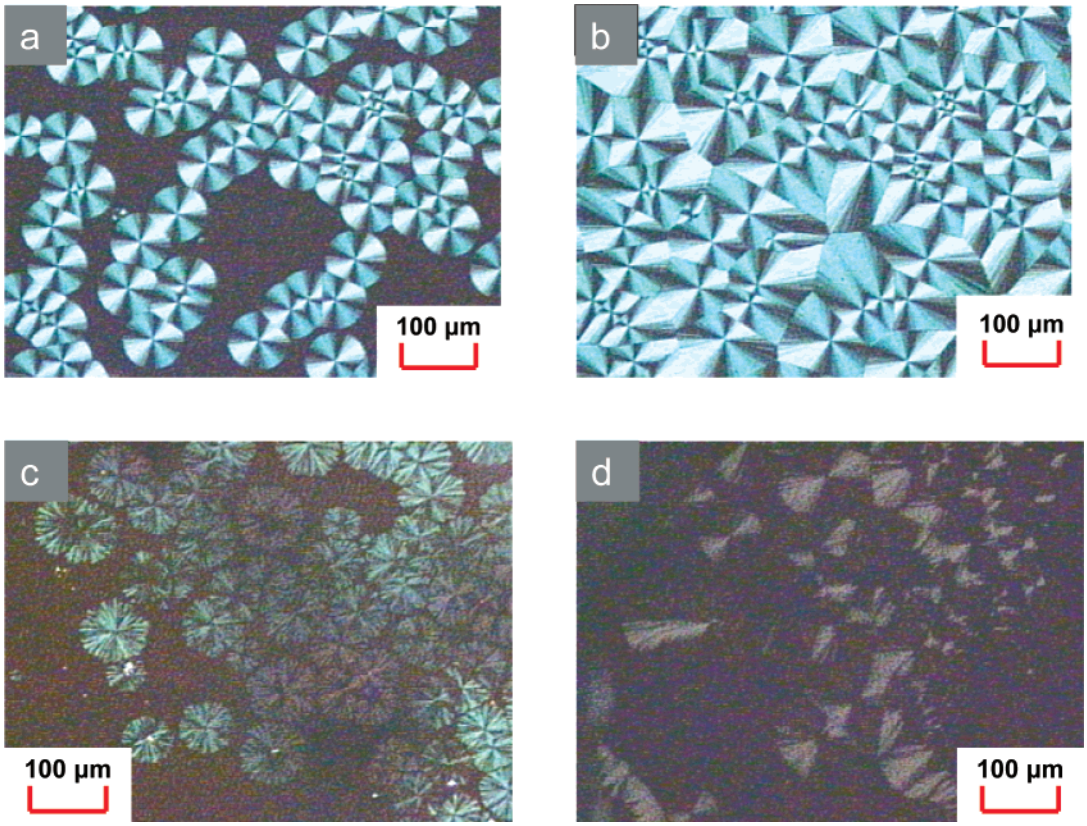

Figure 4. Optical micrographs of poly(MPEGMA) brushes grown from gold surfaces and viewed through crossed polarizers: (a) and (b) show a 240 nm thick film that was heated to 45 °C and cooled to 10 and 5 °C, respectively, at a rate of 1 °C/min; (c) and (d) show 148 and 76 nm thick films that were heated to 45 °C and cooled to 5 °C at a rate of 1 °C/min.

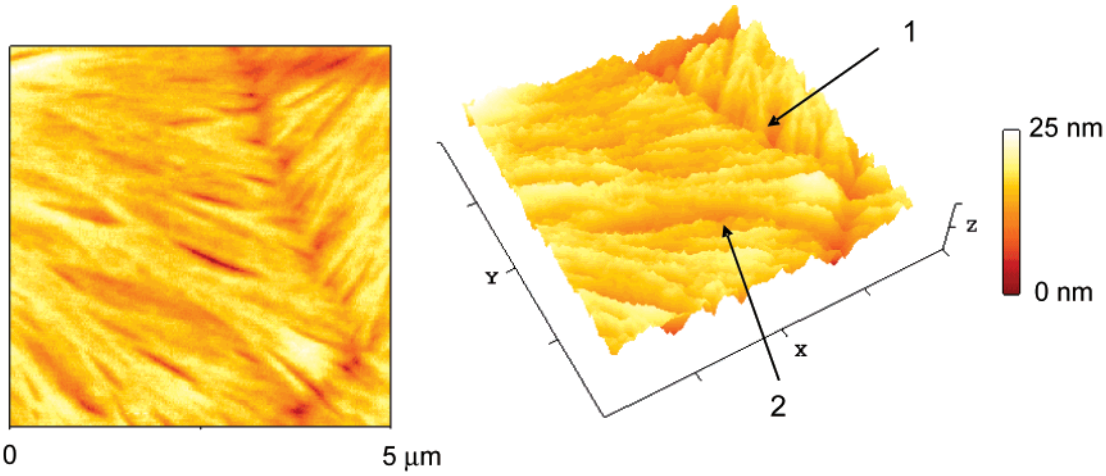

Figure 5. AFM images of a 108 nm thick poly(MPEGMA) film crystallized isothermally at room temperature under N_2 for >24 h. At left is the height image and at right is the corresponding 3-D view. The scan size is 5 × 5 μm, with a z scale of ~25 nm. Arrow 1 identifies the boundary between two spherulites, and arrow 2 indicates the edges of the lamellae.

The evolution of film morphology with thickness was examined using 20−300 nm films crystallized under identical conditions (isothermal crystallization at 23 ± 2 °C for >24 h). Figure 6 shows AFM height images for 122 and 310 nm films. The 310 nm film shows thick, closely packed lamellae oriented perpendicular to the surface. An interesting morphological feature observed in the 122 nm thick film is the branching and curving of lamellae as expected for the radial growth of "spherulites". The morphologies of films with thicknesses <100 nm are more complicated and are thickness-dependent. Surface morphology of 92 and 70 nm thick films are similar, both showing aggregation of lamellae (Figure 7a,b), although the lamellar morphology seen in the height image is less resolved compared to thicker films. A switch from perpendicularly oriented lamellae to lamellae presumably lying parallel to the surface is suggested by the image of a 55 nm film, which shows a wormlike film morphology that resembles aggregates of lamellae oriented parallel to the surface. For the 35 nm thick film, the surface is nearly topologically homogeneous with a root-mean-square roughness of 1.8 nm. Moreover, its featureless phase image (see Supporting Information) also suggests the near-surface structure is amorphous.

Spectroscopic Characterization. Reflectance FT-IR spectroscopy can confirm crystallization as well as provide information on the orientation of the poly(MPEGMA) side chains relative to the surface. As seen in Figure 2, crystallization causes

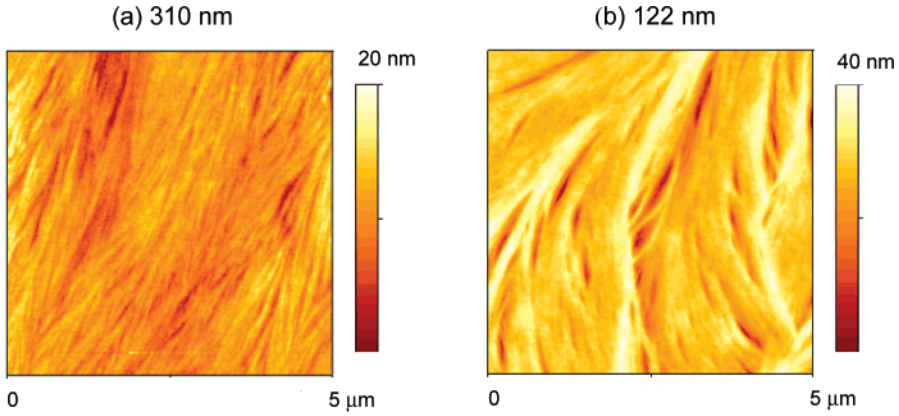

Figure 6. AFM height images (5 × 5 μm) of crystalline poly(MPEGMA) brushes with thicknesses of (a) 310 and (b) 122 nm. The films were crystallized isothermally at room temperature under N_2 for >24 h.

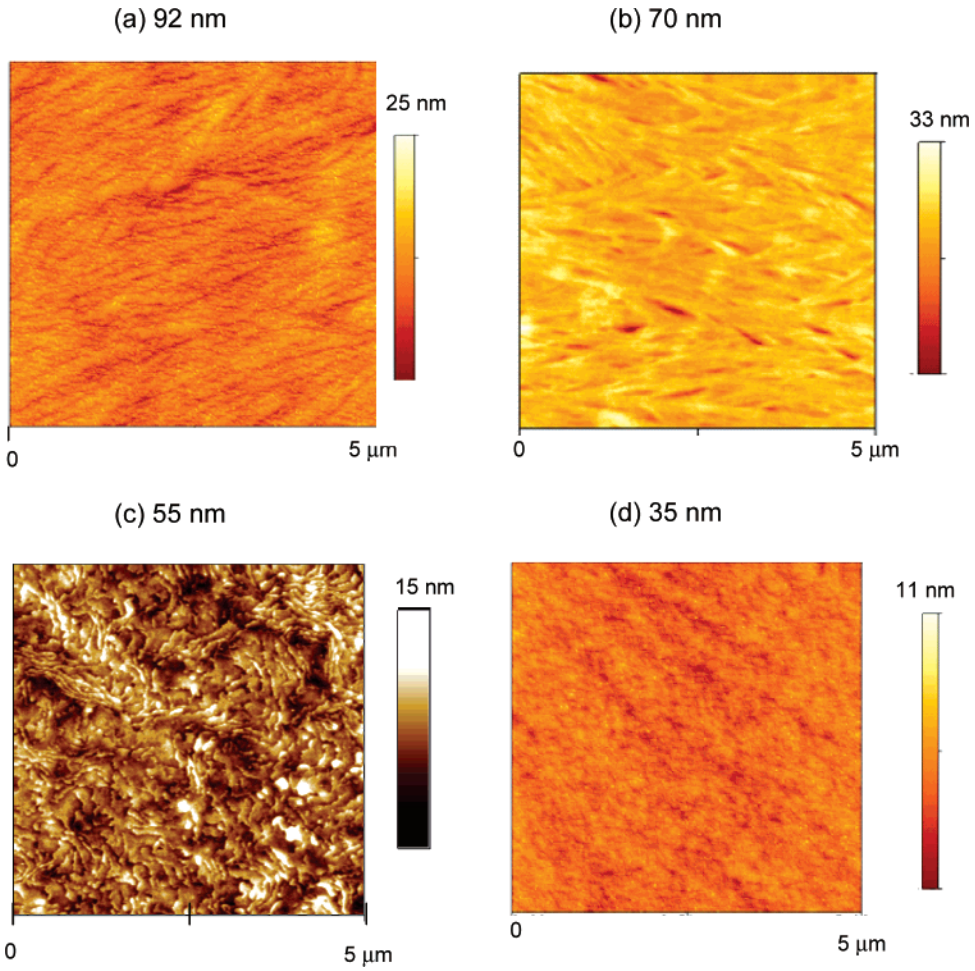

Figure 7. AFM height images (5 × 5 μm) of crystalline poly(MPEGMA) brushes with thicknesses of (a) 92, (b) 76, (c) 55, and (d) 35 nm. (Note that *z*-scales vary among the images.) The films were crystallized isothermally at room temperature under N_2 for >24 h.

several poly(MPEGMA) IR bands to sharpen. Notable changes consistent with crystallization include splitting of the C−O−C band at 1150 cm^{-1} into peaks at 1120 and 1148 cm^{-1} and evolution of the CH_2 wagging peak at ~1350 cm^{-1} into a sharp peak at 1360 cm^{-1} with a small shoulder at 1344 cm^{-1}. Both indicate a high degree of crystallinity for the PEO chain.

Therefore, a series of poly(MPEGMA) brushes with thicknesses ranging from 13 to 240 nm were characterized by reflectance FT-IR spectroscopy (Figure 8). The widths and positions of the peaks in the spectrum of the 13 nm thick film indicate that this brush was amorphous. All films of comparable thickness (<20 nm) proved to be amorphous, possibly because the restricted conformations of ultrathin films prevent efficient packing of the PEO side chains into crystalline lamellae. Alternatively, films <20 nm thick may have melting points at or below room temperature. However, the latter explanation seems unlikely, since polarized optical microscopy shows that a 300 nm film melts at 38 ± 1 °C, and the melting point only decreases to 34 ± 1 °C for an 80 nm film.

PEO usually crystallizes as a 7_2 helix, which contains seven CH_2CH_2O repeat units and two turns in the 19.3 Å between equivalent sites along the helix. The PEO chain in the helix is a succession of nearly *trans* (CCOC), *trans* (COCC), and *gauche* (OCCO) conformations along the chain.[54,55] Thus, many of the

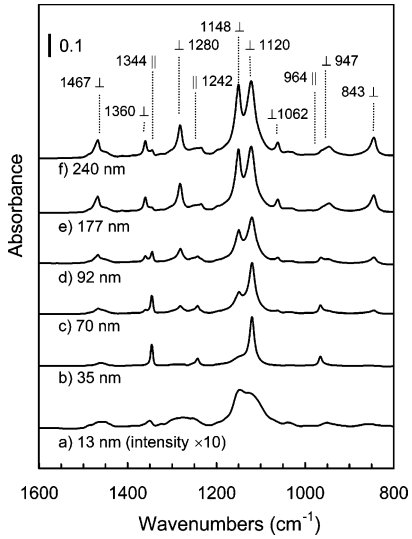

Figure 8. Reflectance FTIR spectra of poly(MPEGMA) brushes with thicknesses of (a) 13, (b) 35, (c) 70, (d) 92, (e) 177, and (f) 240 nm. The brushes were initially annealed at 50 °C and then allowed to crystallize at room temperature in N_2 for >24 h.

Table 1. Absorption Band Assignments for Semicrystalline PEO

band assignment[a]	orientation of transition dipole[b]	wavenumbers (cm^{-1}) (lit. values[c])	wavenumbers (cm^{-1}) (obsd, this work)
$\delta(CH_2)$	⊥	1473, 1466	1467
$\delta(CH_2)$	||	1461, 1453	*d*
$w(CH_2)$	⊥	1358	1360
$w(CH_2)$	||	1342	1344
$t(CH_2)$	⊥	1278	1280
$t(CH_2)$	||	1240	1242
υ(CO)	⊥	1147	1148
υ(CO)	⊥	1116	1120
υ(CO)	||	1103	*e*
υ(CO) + $r(CH_2)$ + υ(CC)	⊥	1060	1062
$r(CH_2) + \upsilon(CH_2)$	||	958	964
$r(CH_2) + \upsilon$(CC)	⊥	947	947
$r(CH_2) + \upsilon$(CO)	⊥	844	843

[a] From refs 42 and 47; δ = scissor; w = wag; t = twist; υ = stretch; r = rock. [b] ⊥ and || represent the direction of transition dipole moments perpendicular and parallel to the helical axis of PEO, respectively. [c] References 42 and 47. [d] Overlapped. [e] Not observed.

PEO IR bands divide into two groups: one with a transition dipole moment parallel to the helical axis and the other with a transition dipole moment perpendicular to the helical axis (Table 1). When helices are preferentially oriented with respect to a conductive substrate, the relative intensities of different reflectance IR bands provide information about the helix orientation. Specifically, only bands with components of their transition dipole moments that are perpendicular to the substrate will be observed.

Because of orientation effects, the reflectance IR spectrum of a 35 nm thick film (Figure 8, spectrum b) shows only four peaks between 1400 and 900 cm^{-1} (1344, 1242, 1120, and 964 cm^{-1}). Absorption bands at 1344, 1242, and 964 cm^{-1} correspond to vibrations with transition moments parallel to the helical axis, while most bands that are perpendicular to the helix were not observed. The bands at 1120 and 1467 cm^{-1} are less sensitive to conformation order (parallel or perpendicular) and appear in all samples. These data strongly suggest that the helical axis of PEO units was oriented perpendicular to the substrate in the 35 nm thick film.

The FT-IR spectra evolved as the film thickness increased, however. Spectrum c (70 nm thick film) in Figure 8 shows a band at 1148 cm^{-1}, which appears as a shoulder of the 1120 cm^{-1} peak. The splitting of this C−O−C absorption confirms crystallization of the ethylene oxide segments. In addition to the 1344 and 1242 cm^{-1} bands seen in thinner films, there are new absorptions in spectrum c at 1360 and 1280 cm^{-1}. These bands are even more obvious in spectrum d (92 nm thick film). The 1360, 1280, 1148, 1062, 947, and 843 cm^{-1} peaks correspond to vibrations with transition moments perpendicular to the helical axis. Thus, there appear to be two populations of helical PEO in the 92 nm thick film: one with its axis perpendicular to the surface and the other parallel to the surface. In thicker films (traces e and f), the 1360, 1280, 947, and 843 cm^{-1} bands dominate the spectrum, indicating an increasing proportion of PEO chains oriented parallel to the surface and, consequently, lamellae oriented perpendicular to the surface.

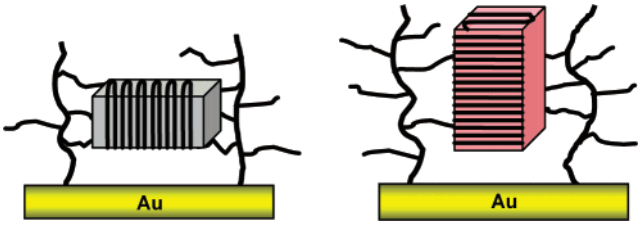

Figure 9. Lamellae orientations in films of poly(MPEGMA). (left) Chain axis of PEO side chains is oriented perpendicular to the substrate resulting in lamellae lying flat on the surface; parallel lamellae orientation. (right) Chain axis of PEO side chains is oriented parallel to the substrate resulting in lamellae oriented normal to the surface; perpendicular lamellae orientation.

The FT-IR data are consistent with the previous interpretations of the AFM images. The morphology of films >100 nm thick appears to be dominated by perpendicularly oriented lamellae, since polarized FT-IR measurements identify the dominant helix orientation in these films as parallel to the surface and hence consistent with lamellae oriented normal to the surface. The morphologies of films <100 nm thick are more complicated, with AFM showing a progressive loss of perpendicular lamellae as films become thinner. For very thin films such as the 35 nm thick film shown in Figure 7, the AFM image was featureless, but FT-IR spectroscopy detected relatively sharp bands at 1342, 1242, 1120, and 964 cm^{-1}, indicating some order and, by inference, some degree of crystallinity. In contrast, the 55 nm film shows signs of structure in the AFM image, but the structure is different than seen in thicker films, suggesting lamellae oriented parallel to the surface. The FT-IR spectra of thin films are consistent with such a conclusion. IR measurements indicate that the PEO chains in the 92 and 70 nm thick films are orientated both parallel and perpendicular to the surface. AFM only showed irregular perpendicular lamellae, possibly due to the overgrowth of perpendicular lamellae on the top of parallel lamellae. In addition, AFM usually detects the top layer morphology of the film, while vibrational bands shown in the IR spectra reflect mean orientations of polymer chains.

The two orientations for crystalline lamellae in poly(MPEGMA) brushes are shown in Figure 9. Rafailovich et al.[56] claimed that for the crystallization of thick LDPE films the energy of the primary nucleation step is minimal when the chains are oriented parallel to the surface. However, since near-simultaneous nucleation of spherulites and preliminary studies of the poly(MPEGMA) crystallization rate as a function of film thickness are consistent with heterogeneous nucleation at defect sites, formation of perpendicular lamellae may be driven by the comblike architecture of poly(MPEGMA), which favors interactions between adjacent side chains when the polymer backbones

are oriented parallel to each other. Bulk comb polymer samples typically crystallize in layers with the crystalline side chains oriented roughly perpendicular to the backbone. Densely packed comb polymer brushes favor an extended polymer backbone when the surface density is high enough, with the polymer backbones roughly oriented perpendicular to the surface and the side chains parallel to the surface. Crystal growth follows the same orientation, leading to the perpendicular lamellae. A similar side-chain orientation was described recently by Gabriel et al.[57]

In addition to identifying chain orientation, reflectance FT-IR spectroscopy suggests that films must be >20 nm thick to exhibit detectable crystallinity. Several groups studied spin-coated PEO films and reported different results regarding the critical film thickness for crystallization. Schönherr et al.[5] did not observe crystallinity in films <15 nm. However, Reiter et al.[12,58] reported crystallization in monolayer-thick films (~5 nm). The poly(MPEGMA) case is structurally different from spin-coated PEO because the backbones of comblike structures usually interfere with crystallization of side-chain segments adjacent to the polymer backbone, and this should lead to a higher critical thickness for crystallization than in linear PEO films. We note that T_m of the poly(MPEGMA) brushes is significantly lower than those for linear PEO, which suggests a lower thermodynamic stability. In addition, polymer brushes with high graft densities may be viewed as preorganized for crystallization, but more restricted in terms of available chain conformations. More detailed studies of the crystallization rates will illuminate the importance of these issues.

Summary

Semicrystalline polymer brushes were grown from gold-coated substrates using surface-initiated ATRP of MPEGMA macromonomers in water. The PEO side chains of these comb polymers crystallized at room temperature to give a two-dimensional spherulitic morphology, and the degree of crystallization decreased with decreasing film thickness. In addition, the orientation of crystalline lamellae in the films is also film thickness dependent. Both AFM and IR data are consistent with lamellae oriented perpendicular to the substrate for films with thicknesses over 100 nm, i.e., helical axis of PEO side chains is parallel to the surface; while thinner films likely show a preference for lamellae oriented parallel to the surface.

Acknowledgment. The authors thank NSF Center for Sensor Materials at Michigan State University for financial support. M.L.B. acknowledges funding from the Department of Energy, Office of Basic Energy Sciences. We also thank Professor Michael Mackey and Tiffany Dukette (MSU) for access to and help with AFM.

Supporting Information Available: AFM phase images of 35 and 92 nm crystalline polymer brushes (Figure S1). This material is available free of charge via the Internet at http://pubs.acs.org.

References and Notes

(1) Senaratne, W.; Andruzzi, L.; Ober, C. K. *Biomacromolecules* **2005**, *6*, 2427−2448.
(2) Zhou, F.; Huck, W. T. S. *Phys. Chem. Chem. Phys.* **2006**, *8*, 3815−3823.
(3) Frank, C. W.; Rao, V.; Despotopoulou, M. M.; Pease, R. F. W.; Hinsberg, W. D.; Miller, R. D.; Rabolt, J. F. *Science* **1996**, *273*, 912−915.
(4) Prucker, O.; Christian, S.; Bock, H.; Ruhe, J.; Frank, C. W.; Knoll, W. *Org. Thin Films* **1998**, *695*, 233−249.
(5) Schönherr, H.; Frank, C. W. *Macromolecules* **2003**, *36*, 1188−1198.
(6) Schönherr, H.; Frank, C. W. *Macromolecules* **2003**, *36*, 1199−1208.
(7) Pearce, R.; Vancso, G. J. *Macromolecules* **1997**, *30*, 5843−5848.
(8) Pearce, R.; Vancso, G. J. *Polymer* **1998**, *39*, 1237−1242.
(9) Mellbring, O.; Oiseth, S. K.; Krozer, A.; Lausmaa, J.; Hjertberg, T. *Macromolecules* **2001**, *34*, 7496−7503.
(10) Sakai, Y.; Imai, M.; Kaji, K.; Tsuji, M. *Macromolecules* **1996**, *29*, 8830−8834.
(11) Wang, M. T.; Braun, H. G.; Meyer, E. *Macromolecules* **2004**, *37*, 437−445.
(12) Reiter, G.; Sommer, J. U. *J. Chem. Phys.* **2000**, *112*, 4376−4383.
(13) Despotopoulou, M. M.; Frank, C. W.; Miller, R. D.; Rabolt, J. F. *Macromolecules* **1995**, *28*, 6687−6688.
(14) Despotopoulou, M. M.; Frank, C. W.; Miller, R. D.; Rabolt, J. F. *Macromolecules* **1996**, *29*, 5797−5804.
(15) Hu, Z. J.; Huang, H. Y.; Zhang, F. J.; Du, B. Y.; He, T. B. *Langmuir* **2004**, *20*, 3271−3277.
(16) Dalnoki-Veress, K.; Forrest, J. A.; Massa, M. V.; Pratt, A.; Williams, A. *J. Polym. Sci., Part B: Polym. Phys.* **2001**, *39*, 2615−2621.
(17) Mareau, V. H.; Prud'homme, R. E. *Macromolecules* **2005**, *38*, 398−408.
(18) Marentette, J. M.; Brown, G. R. *Polymer* **1998**, *39*, 1405−1414.
(19) Massa, M. V.; Dalnoki-Veress, K.; Forrest, J. A. *Eur. Phys. J. E* **2003**, *11*, 191−198.
(20) Schultz, J. M.; Miles, M. J. *J. Polym. Sci., Part B: Polym. Phys.* **1998**, *36*, 2311−2325.
(21) Taguchi, K.; Miyaji, H.; Izumi, K.; Hoshino, A.; Miyamoto, Y.; Kokawa, R. *Polymer* **2001**, *42*, 7443−7447.
(22) Zdyrko, B.; Klep, V.; Luzinov, I. *Langmuir* **2003**, *19*, 10179−10187.
(23) Zdyrko, B.; Varshney, S. K.; Luzinov, I. *Langmuir* **2004**, *20*, 6727−6735.
(24) Coca, S.; Jasieczek, C. B.; Beers, K. L.; Matyjaszewski, K. *J. Polym. Sci., Polym. Chem.* **1998**, *36*, 1417−1424.
(25) Perrier, S.; Haddleton, D. M. *Macromol. Symp.* **2002**, 261−272.
(26) Coullerez, G.; Carlmark, A.; Malmstrom, E.; Jonsson, M. *J. Phys. Chem. A* **2004**, *108*, 7129−7131.
(27) Matyjaszewski, K.; Xia, J. H. *Chem. Rev.* **2001**, *101*, 2921−2990.
(28) Sarbu, T.; Pintauer, T.; McKenzie, B.; Matyjaszewski, K. *J. Polym. Sci., Part A: Polym. Chem.* **2002**, *40*, 3153−3160.
(29) Wang, X. S.; Armes, S. P. *Macromolecules* **2000**, *33*, 6640−6647.
(30) Wang, X. S.; Lascelles, S. F.; Jackson, R. A.; Armes, S. P. *Chem. Commun.* **1999**, 1817−1818.
(31) Wang, X. S.; Malet, F. L. G.; Armes, S. P.; Haddleton, D. M.; Perrier, S. *Macromolecules* **2001**, *34*, 162−164.
(32) Jones, D. M.; Brown, A. A.; Huck, W. T. S. *Langmuir* **2002**, *18*, 1265−1269.
(33) Jones, D. M.; Huck, W. T. S. *Adv. Mater.* **2001**, *13*, 1256−1259.
(34) Edmondson, S.; Osborne, V. L.; Huck, W. T. S. *Chem. Soc. Rev.* **2004**, *33*, 14−22.
(35) Huang, W. X.; Baker, G. L.; Bruening, M. L. *Angew. Chem., Int. Ed.* **2001**, *40*, 1510.
(36) Huang, W. X.; Kim, J. B.; Bruening, M. L.; Baker, G. L. *Macromolecules* **2002**, *35*, 1175−1179.
(37) Neugebauer, D.; Theis, M.; Pakula, T.; Wegner, G.; Matyjaszewski, K. *Macromolecules* **2006**, *39*, 584−593.
(38) Inomata, K.; Nakanishi, E.; Sakane, Y.; Koike, M.; Nose, T. *J. Polym. Sci., Part B: Polym. Phys.* **2005**, *43*, 79−86.
(39) Lin, H.; Wagner, E. V.; Freeman, B. D.; Toy, L. G.; Gupta, R. *Science* **2006**, *311*, 639−642.
(40) Andrade, J. D.; Hlady, V.; Jeon, S.-I. In *Hydrophilic Polymers*; Advances in Chemistry Series 248; American Chemical Society: Washington, DC, 1996; pp 51−59.
(41) *Polyethylene glycol*: *Chemistry and Biological Applications*; Harris, J. M., Zalipsky, S., Eds.; ACS Symposium Series 680; American Chemical Society: Washington, DC, 1997; 489 pgs.
(42) Yoshihara, T.; Murahashi, S.; Tadokoro, H. *J. Chem. Phys.* **1964**, *41*, 2902.
(43) Miyazawa, T.; Ideguchi, Y.; Fukushima, K. *J. Chem. Phys.* **1962**, *37*, 2764.
(44) Sun, X.; Zhang, H.; Zhang, L.; Wang, X.; Zhou, Q.-F. *Polym. J.* **2005**, *37*, 102−108.
(45) Richardson, P. H.; Richards, R. W.; Blundell, D. J.; MacDonald, W. A.; Mills, P. *Polymer* **1995**, *36*, 3059−69.
(46) Wang, M. T.; Braun, H. G.; Meyer, E. *Polymer* **2003**, *44*, 5015−5021.
(47) Hoffmann, C. L.; Rabolt, J. F. *Macromolecules* **1996**, *29*, 2543−2547.
(48) Inomata, K.; Sasaki, Y.; Nose, T. *J. Polym. Sci., Part B: Polym. Phys.* **2002**, *40*, 1904−1912.

(49) Shah, R. R.; Merreceyes, D.; Husemann, M.; Rees, I.; Abbott, N. L.; Hawker, C. J.; Hedrick, J. L. *Macromolecules* **2000**, *33*, 597−605.
(50) MacCallum, J. R.; Vincent, C. A. *Polymer Electrolyte Reviews-1*; Elsevier Science Publishing Co.: New York, 1987.
(51) Nomura, E.; Ito, K.; Kajiwara, A.; Kamachi, M. *Macromolecules* **1997**, *30*, 2811−2817.
(52) Ma, H. W.; Wells, M.; Beebe, T. P.; Chilkoti, A. *Adv. Funct. Mater.* **2006**, *16*, 640−648.
(53) Feng, W.; Chen, R.; Brash, J. L.; Zhu, S. *Macromol. Rapid Commun.* **2005**, *26*, 1383−1388.
(54) Miyazawa, T.; Ideguchi, Y.; Fukushima, K. *J. Chem. Phys.* **1962**, *37*, 2764−&.
(55) Yoshihara, T.; Murahashi, S.; Tadokoro, H. *J. Chem. Phys.* **1964**, *41*, 2902.
(56) Wang, Y.; Ge, S.; Rafailovich, M.; Sokolov, J.; Zou, Y.; Ade, H.; Luning, J.; Lustiger, A.; Maron, G. *Macromolecules* **2004**, *37*, 3319−3327.
(57) Gabriel, S.; Dubruel, P.; Schacht, E.; Jonas, A. M.; Gilbert, B.; Jerome, R.; Jerome, C. *Angew. Chem., Int. Ed.* **2005**, *44*, 5505−5509.
(58) Reiter, G.; Sommer, J. U. *Phys. Rev. Lett.* **1998**, *80*, 3771−3774.

MA070367P